A Triple-Memristor Hopfield Neural Network With Space Multi-Structure Attractors And Space Initial-Offset Behaviors

Hairong Lin, *Member, IEEE*, Chunhua Wang, Fei Yu, Qinghui Hong, Cong Xu, and Yichuang Sun, *Senior Member, IEEE*

***Abstract*—Memristors have recently demonstrated great promise in constructing memristive neural networks with complex dynamics. This paper proposes a memristive Hopfield neural network with three memristive coupling synaptic weights. The complex dynamical behaviors of the triple-memristor Hopfield neural network (TM-HNN), which have never been observed in previous Hopfield-type neural networks, include space multi-structure chaotic attractors and space initial-offset coexisting behaviors. Bifurcation diagrams, Lyapunov exponents, phase portraits, Poincar*é* maps, and basins of attraction are used to reveal and examine the specific dynamics. Theoretical analysis and numerical simulation show that the number of space multi-structure attractors can be adjusted by changing the control parameters of the memristors, and the position of space coexisting attractors can be changed by switching the initial states of the memristors. Extreme multistability emerges as a result of the TM-HNN's unique dynamical behaviors, making it more suitable for applications based on chaos. Moreover, a digital hardware platform is developed and the space multi-structure attractors as well as the space coexisting attractors are experimentally demonstrated. Finally, we design a pseudo-random number generator to explore the potential application of the proposed TM-HNN.**

***Index Terms*—Hopfield neural network (HNN), memristor synapse, multi-structure attractor, initial-offset behavior, coexisting attractors, field-programmable gate array (FPGA) implementation**

I. Introduction

BIOLOGICAL brain is a highly complex nonlinear system with chaotic dynamical behaviors [1, 2]. Artificial neural networks have received a lot of attention for their design and research in an effort to imitate the structure and characteristics of the biological brain [3, 4]. Among them, Hopfield neural network (HNN) with brain-like network structure and brain-like dynamics is an especially significant model [5]. On one hand, some brain functions can be well understood through the study of the dynamics of the HNN, for example, memory [6], neuroregulation [7], and so on [8]. On the other hand, the HNN with complex dynamics can be widely applied in the field of artificial intelligence to solve practical issues, such as pattern recognition [9], image processing [10], as well as combinatorial optimization [11]. Over the past few decades, an enormous number of improved HNN models have emerged to generate complex dynamical behaviors such as chaos [12], coexisting behaviors [13], and synchronization [14]. These research results not only help to further understand how the brain works, but also to promote the development of artificial intelligence.

Based on the symmetry theory of fundamental circuit variables, Chua proposed the memristor concept in 1971 [15]. Hewlett-Packard Lab produced the first physical memristor successfully in 2008 [16], which significantly increased applications of memristors. The unique nonvolatility and nonlinearity of the memristor, which bridges the gap between charge and flux, makes it a novel circuit element [17]. Last twenty years, the memristor has been widely applied to construct memristive chaotic systems [18] and memristive neural networks [19-21]. Especially, it can be used to build memristive Hopfield neural networks (MHNNs) [22, 23], which makes the artificial neural networks closer to the biological brain. On one hand, the memristor can be used to describe electromagnetic induction effect in biological nervous systems because of its characteristic of magnetic flux. Under electromagnetic radiation, for instance, the MHNNs can be constructed using the HNNs [24, 25]. Furthermore, memristive electromagnetic induction effects between neurons can also be used to model the MHNNs [26, 27]. The memristor, on the other hand, is typically used to emulate biological synapses due to its unique nonlinearity and nonvolatility. For example, memristor synapses can be used to replace resistor synapses in HNNs to create MHNNs [28-30]. Numerous MHNN models based on these strategies have been proposed over the past ten years. The MHNNs have been found to have a variety of complex dynamical behaviors, such as hyperchaos [31], hidden attractors [32], chimera [33], and multistability [34, 35].

Recently, several works on complex multi-scroll attractors have been reported in the MHNNs. Multi-scroll attractors are complex chaotic behaviors [36, 37], which have special scroll trajectories. Compared with single-scroll attractors, multi-scroll attractors have higher adjustability and complexity. The multi-scroll dynamics of the MHNN, for example, has been first revealed in Ref. [38]. The authors found four-scroll and six-scroll attractors after investigating the effect on the dynamical behaviors of the neural network under electromagnetic radiation. Multi-double-scroll attractors in the MHNN have been reported in Ref. [39]. In an HNN with three neurons, the authors demonstrated that the memristive self-

Manuscript received Jan 18, 2023; This work is supported by the National Natural Science Foundation of China (62201204, 62271197, 61971185, 62001163), the China Postdoctoral Science Foundation (2022M71104), the Natural Science Foundation of Hunan Province (2023JJ40168). (*Corresponding author: Chunhua Wang.*)

Hairong Lin, Chunhua Wang and Qinghui Hong are with the College of Computer Science and Electronic Engineering, Hunan University, Changsha, 410082, China. (haironglin@hnu.edu.cn; wch1227164@hnu.edu.cn)

Fei Yu and Cong Xu are with School of Computer and Communication Engineering in Changsha University of Science and Technology, Changsha, 410114, China.

Yichuang Sun is with the School of Engineering and Computer Science, University of Hertfordshire, Hatfield AL10 9AB, U.K.

connection synaptic weight can encourage the formation of multiple double-scroll attractors. Besides, plane multi-scroll attractors have been observed from an MHNN with two memristor synapses [40]. In the meantime, some similar multi-scroll MHNNs have been proposed and successfully applied in the information security field [41-43]. More recently, Ref. [44] proposed an MHNN which can generate multi-structure chaotic attractors that are more complex than multi-scroll attractors. However, the MHNN realized only single-directional multi-structure chaotic attractors. Is it possible to achieve plane or space multi-structure attractors in an MHNN?

Additionally, the work on initial-offset behavior in the MHNNs has become a hot topic. Following multistability and extreme multistability, a new type of complex dynamics is the initial-offset behavior [45, 46]. It refers to the existence of an infinite number of attractors with identical topologies but distinct positions. In particular, the initial-offset behavior has the potential to produce stable and robust chaotic sequences with oscillating amplitudes that can be non-destructively controlled by flexibly switching initial states. In Ref. [47], the initial-offset behavior of the MHNN has been examined. Line initial-offset coexisting attractors can be seen in the MHNN with a single memristive self-connection synaptic weight, according to the findings of the study. Ref. [48] demonstrates that the MHNN with a single memristor synapse can produce hidden chaotic attractors with identical initial offsets. And the dynamics of initial-offset coexisting hyperchaotic attractors have been revealed in a coupled MHNN [49]. Furthermore, in Ref. [50], the plane initial-offset coexisting behaviors in the MHNN have been discovered. The authors demonstrated that two memristive self-connected synaptic weights can make the HNN with two neurons produce plane initial-offset coexisting attractors. Space initial-offset behaviors in the MHNN have not yet been documented, however.

Drawing inspiration from the above analyses, this paper presents a triple-memristor HNN (TM-HNN), which is constructed by substituting three resistive coupling synaptic weights with three memristive coupling synaptic weights. Wonderfully, the TM-HNN not only can exhibit space multi-structure attractors by adjusting the memristors' control parameters, but also can exhibit space initial-offset behavior by switching the memristors' initial states. As far as the authors know, the space multi-structure attractors and the space initial-offset behavior in the HNN have not been reported in the literature.

This article's novelty and major contributions can be summarized as follows:(1) We design a multistable locally active memristor and propose a TM-HNN with four neurons. Unlike other MHNN models, the TM-HNN is constructed considering three memristive coupling synaptic weights. (2) The space multi-structure attractors and space initial-offset coexisting behaviors are demonstrated through theoretical analysis and numerical methods. Emphatically, by altering the control parameters and initial conditions of the memristors, respectively, one can conveniently control the number of space multi-structure attractors and the position of the space initial-offset coexisting attractors. (3) A FPGA-based hardware platform is developed and the space multi-structure attractors and space initial-offset coexisting attractors are experimentally reproduced. Experimental results show that the TM-HNN is capable of producing highly random numbers.

The following is how the rest of this paper is laid out. Section II designs a multistable locally active memristor and presents a TM-HNN model. Section III investigates the space multi-structure attractors and the space initial-offset behavior. The hardware platform based on an FPGA is made to check the numerical results in Section IV. Finally, Section V concludes with a few conclusions.

II. Description of Triple-Memristor Hopfield Neural Network

First, a multistable locally active memristor model is designed in this section. The designed memristor is then used to construct a triple-memristor Hopfield neural network.

A. Design Of Multistable Locally Active Memristor

Memristors with nature nonlinearity and memory are typically accustomed to emulating neural synapses. Recently, Lai et al. [41] designed a robust hyperbolic tangent memristor to simulate the neural synapse in a memristive neural network. Due to its adjustable parameters, this memristor has significantly more adjustability and diversity than other memristor models. Unfortunately, the memristor is not locally active. Inspired by this memristor model, we design a multistable locally active memristor as follows

$$\begin{cases} i = W(\varphi)v = b\varphi v \\ \mathrm{d}\varphi/\mathrm{d}t = cv - dh(\varphi) \end{cases}, \tag{1}$$

where $h(\varphi)$ contains two parts $h_1(\varphi)$ and $h_2(\varphi)$:

$$h_1(\varphi)=\begin{cases} \varphi, N=0 \\ \varphi-\sum\limits_{i=1}^{N}(\tanh(p(\varphi+(2i-1)))+\tanh(p(\varphi-(2i-1)))) \\ N=1,2,3,\ldots \end{cases} \tag{2}$$

$$h_2(\varphi)=\begin{cases} \varphi-\tanh(p\varphi), M=0 \\ \varphi-\tanh(p\varphi)-\sum\limits_{j=1}^{M}(\tanh(p(\varphi+2j))+\tanh(p(\varphi-2j))) \\ M=1,2,3,\ldots \end{cases} \tag{3}$$

where b, c, and d are three memristor parameters, p=10^4 is a fixed coefficient, and N, M are two control parameters. The intrinsic properties including pinched hysteresis loop, nonvolatility, multistability, and local activity of the designed memristor are analyzed as follows. Setting b=0.01, and c=d=1, taking M=2 as an example, when a sinusoidal voltage $v = A\sin(2\pi Ft)$ with signal amplitudes A=8 and different signal frequencies F (10, 20, 100) is applied in the memristor, it exhibits classical pinched hysteresis loop on the $v-i$ plane, as shown in Fig.1(a). Especially, with the increase in frequency, the area of the pinched hysteresis loop of the memristor decreases gradually, which implies that the proposed model is a memristor device.

According to the memristor theory [51], the power-off plot (POP) can be used to verify the nonvolatility of the memristor. For the memristor state equation in equation (1), let v=0, it can be reduced as

$$\mathrm{d}\varphi/\mathrm{d}t = -dh(\varphi). \tag{4}$$

The dynamic route of the dynamical equation (4), namely POP, is drawn in Fig.1(b). As we can see, when $\mathrm{d}\varphi/\mathrm{d}t$=0,

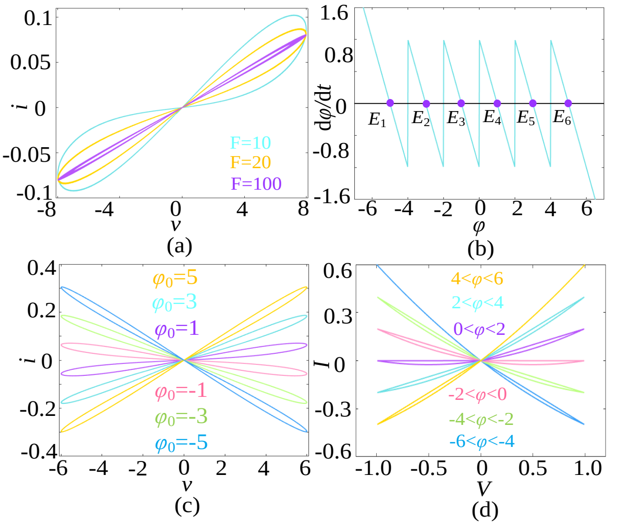

Fig. 1: Characteristics of the multistable locally active memristor with b=0.01, c=d=1, p=10^4, and M=2. (a) Pinched hysteresis loops related to frequency, where A=8, φ_0=0. (b) POP. (c) Pinched hysteresis loops related to initial states, where A=6, F=10. (d) DC V-I loci.

there are six stable equilibrium points (E_1-E_6) with a negative slope. Therefore, the designed memristor has the characteristic of non-volatile memory. Meanwhile, the memristor can exhibit coexisting six pinched hysteresis loops with A=6, F=10, and different initial values (-5, -3, -1, 1, 3, 5), as shown in Fig.1(c). In fact, further study shows that the memristor can generate coexisting (2N+1) or (2M+2) pinched hysteresis loops, which means that the designed memristor is multistable. The local activity of the designed memristor can be proved by using the direct current voltage-current (DC V-I) loci [51]. In equation (1), letting dφ/dt=0, it can be rewritten as

$$\begin{cases} I = b\varphi V \\ V = dh(\varphi)/c \end{cases} . \tag{5}$$

where V and I denote input DC voltage and output DC current. Considering equation (5), the input voltage V value changes from -1.2 V to 1.2 V and the variable φ value varies within [-6, 6], the DC V-I loci of the memristor can be derived, as shown in Fig.1(d). From Fig.1(d), when the state variable $\varphi < 0$, the slope of the V-I loci is negative, which shows that the designed memristor is locally active. To sum up, the designed multistable locally active memristor has synapse-like features of multistability, non-volatile memory, and local activity, which means that it is very appropriate for emulating neural synapses.

B. Construction Of Triple-Memristor Hopfield Neural Network

Hopfield neural networks are widely studied because of their brain-like network structure and complicated chaotic dynamics. It can be described by a set of differential equations: [5]

$$C_i\dot{x}_i = -\frac{x_i}{R_i} + \sum_{j=1}^{n} w_{ij}\tanh(x_j) + I_i \quad (i, j \in N^*), \tag{6}$$

where x_i, C_i, and R_i represent the membrane voltage, membrane capacitance, and membrane resistance of the i-th neuron, respectively. Besides, tanh(.) and I_i are the neuron activation function and external input current, respectively. w_{ij} denotes synaptic weight between neuron i and neuron j. Usually, the synaptic weight is a resistive synaptic weight that is realized by a resistor. When the resistor is replaced with a memristor, the synaptic weight becomes a memristive synaptic weight and a memristive neural network can be constructed thereby [23]. According to this strategy, a TM-HNN is constructed by using three memristive synaptic weights to substitute three resistive synaptic weights in a four-neuron-based HNN, as shown in Fig.2. Where the memristive synaptic weights are realized with the designed multistable locally active memristors. Combined with the original HNN model (6) with R_i=1, C_i=1, and I_i=0 (i=1, 2, 3, and 4), the mathematical model of the TM-HNN can be described as follows

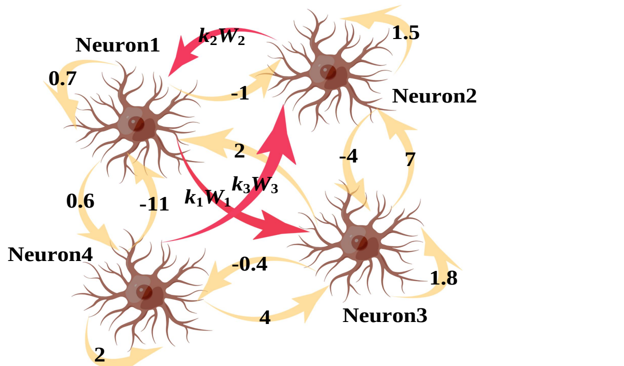

Fig. 2: Connection structure for the TM-HNN.

$$\begin{cases} \dot{x}_1 = -x_1 + 0.7\tanh(x_1) + k_2W_2(\varphi_2)\tanh(x_2) + 2\tanh(x_3) - 11\tanh(x_4) \\ \dot{x}_2 = -x_2 - \tanh(x_1) + 1.5\tanh(x_2) + 7\tanh(x_3) + k_3W_3(\varphi_3)\tanh(x_4) \\ \dot{x}_3 = -x_3 + k_1W_1(\varphi_1)\tanh(x_1) - 4\tanh(x_2) + 1.8\tanh(x_3) + 4\tanh(x_4) \\ \dot{x}_4 = -x_4 + 0.6\tanh(x_1) - 0.4\tanh(x_3) + 2\tanh(x_4) \\ \dot{\varphi}_1 = c_1\tanh(x_1) - d_1h_1(\varphi_1) \\ \dot{\varphi}_2 = c_2\tanh(x_2) - d_2h_2(\varphi_2) \\ \dot{\varphi}_3 = c_3\tanh(x_4) - d_3h_3(\varphi_3) \end{cases} \tag{7}$$

where W_1, W_2, and W_3 are three memristive coupling synaptic weights, k_1, k_2, and k_3 are three coupling coefficients, and c_1, c_2, c_3, d_1, d_2, and d_3 are parameters of the memristor synapses.

III. Investigation of Dynamical Behaviors

The study on dynamical behaviors of artificial neurons and neural networks is significant to better understand brain functions and to develop new neuromorphic systems [52-54]. This section analyzes the dynamical behaviors of the TM-HNN, including distribution and stability for the equilibrium points, reveals the space multi-structure chaotic attractors, and investigates the space initial-offset behavior.

A. Distribution And Stability Of Equilibrium Points

Letting equation (7) equal to 0, the equilibrium points of the TM-HNN can be solved by calculating the following equation

$$\begin{cases} -x_1 + 0.7\tanh(x_1) + k_2W_2(\varphi_2)\tanh(x_2) + 2\tanh(x_3) - 11\tanh(x_4) = 0 \\ -x_2 - \tanh(x_1) + 1.5\tanh(x_2) + 7\tanh(x_3) + k_3W_3(\varphi_3)\tanh(x_4) = 0 \\ -x_3 + k_1W_1(\varphi_1)\tanh(x_1) - 4\tanh(x_2) + 1.8\tanh(x_3) + 4\tanh(x_4) = 0 \\ -x_4 + 0.6\tanh(x_1) - 0.4\tanh(x_3) + 2\tanh(x_4) = 0 \\ c_1\tanh(x_1) - d_1h_1(\varphi_1) = 0 \\ c_2\tanh(x_2) - d_2h_2(\varphi_2) = 0 \\ c_3\tanh(x_4) - d_3h_3(\varphi_3) = 0 \end{cases} \tag{8}$$

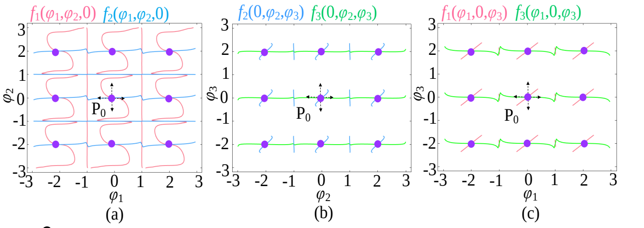

Fig. 3: Distribution of equilibrium points of the TM-HNN with N_1=N_2=N_3=1. (a) φ_1-φ_2 plane. (b) φ_2-φ_3 plane. (c) φ_1-φ_3 plane.

Obviously, equation (8) is difficult to solve with common methods because of its higher-order characteristics. Thus, the solutions will be obtained by using the graphic analysis method. First, equation (8) is changed as

$$\begin{cases} x_1 = \operatorname{atanh}(d_1 h_1(\varphi_1)/c_1) \\ x_2 = \operatorname{atanh}(d_2 h_2(\varphi_2)/c_2) \\ x_4 = \operatorname{atanh}(d_3 h_3(\varphi_3)/c_3) \\ x_3 = \operatorname{atanh}((x_1 - 0.7\tanh(x_1) - k_2 W_2(\varphi_2) + 11\tanh(x_4))/2) \\ f_1(\varphi_1,\varphi_2,\varphi_3) = -x_2 - \tanh(x_1) + 1.5\tanh(x_2) + 7\tanh(x_3) \\ \qquad + k_3 W_3(\varphi_3)\tanh(x_4) \\ f_2(\varphi_1,\varphi_2,\varphi_3) = -x_3 + k_1 W_1(\varphi_1)\tanh(x_1) - 4\tanh(x_2) \\ \qquad + 1.8\tanh(x_3) + 4\tanh(x_4) \\ f_3(\varphi_1,\varphi_2,\varphi_3) = -x_4 + 0.6\tanh(x_1) - 0.4\tanh(x_3) + 2\tanh(x_4) \end{cases} \tag{9}$$

Then, the parameters are set to b=0.01, c_1=2.42, c_2=4.75, c_3=1.3, d_1=2.42, d_2=4.736, d_3=0.6, k_1=2, k_2=1, and k_3=-0.1, respectively. Taking N_1=N_2=N_3=1 as an example, according to equation (9), the distribution of the equilibrium points on the φ_1-φ_2, φ_2-φ_3, and φ_1-φ_3 planes are drawn in Fig.3(a), (b), and (c), respectively. As we can see, each phase plane has nine equilibrium points. Namely, the TM-HNN has 27 equilibrium points. It should be noted that there are some non-equilibrium point intersections due to the boundedness of the hyperbolic tangent function. From the distribution of equilibrium points, the equilibrium point P_0 is synchronously extended along the φ_1-axis, φ_2-axis, and φ_3-axis, respectively. That is to say, with the increase of control parameters N_i and M_i, the number of equilibrium points will be extended along multiple directions including φ_1-axis, φ_2-axis, and φ_3-axis. The number of equilibrium points is determined by further investigation to be equal to ((2N_1+1) or (2M_1+2))×((2N_2+1) or (2M_2+2))×((2N_3+1) or (2M_3+2)). In addition, numerical calculations show that all the equilibrium points are unstable saddle-focus equilibrium points, which means that the TM-HNN can generate self-excited chaotic attractors. Notably, the increase of the control parameters in the TM-HNN leads to the extension of the equilibrium points, which could generate the phenomenon of chaotic attractor reconstruction.

B. Parameter-Related Space Multi-Structure Attractors

The phenomenon of the space multi-structure chaotic attractors is demonstrated by using bifurcation diagrams, Lyapunov exponents, phase portraits, and Poincare maps. Taking N_1=N_2=N_3=0 as a basic example, setting k_1=2, k_2=1, k_3=-0.1, c_1=2.42, c_2=4.75, c_3=1.3, d_1=2.42, d_2=4.736, d_3=0.6, and initial states (x_{10}, x_{20}, x_{30}, x_{40}, φ_{10}, φ_{20}, φ_{30})=(0.1, 0.1, 0.1, 0.1, 0.1, 0.1, 0.1), the bifurcation diagram related to parameter b is plotted in Fig.4(a). As can be seen from the bifurcation diagram, the TM-HNN generates chaotic behavior in three discontinuous intervals, namely, $b\in$[0, 0.2], $b\in$[0.24,0.25], and $b\in$[0.29, 0.46]. The corresponding Lyapunov exponents are shown in Fig.4(b), which further verifies the chaos characteristics. Meanwhile, by selecting b=0.01, a self-excited chaotic attractor with complex structure can be generated from the TM-HNN, as shown in Fig.5. The phase portraits in Fig.5 directly show that the self-excited chaotic attractor has a complex non-scroll/wing structure. So, it is known as a chaotic attractor with a single structure. There is no doubt that an attractor with multiple single structures is considered a multi-structure attractor.

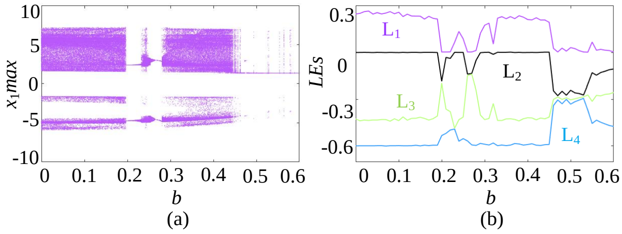

Fig. 4: Dynamical behaviors related to parameter b, where N_1=N_2=N_3=0. (a) Bifurcation diagram. (b) Lyapunov exponents (LEs).

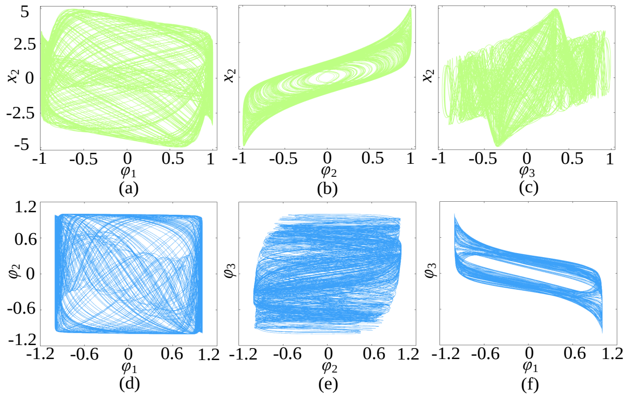

Fig. 5: Single-structure chaotic attractor on different phase planes, where N_1=N_2=N_3=0. (a) φ_1-x_2 plane. (b) φ_2-x_2 plane. (c) φ_3-x_2 plane. (d) φ_1-φ_2 plane. (e) φ_2-φ_3 plane. (f) φ_1-φ_3 plane.

Interestingly, with the increase of the control parameters N_i/M_i, the single-structure chaotic attractor is reconstructed along φ_1-, φ_2-, and φ_3-axes, respectively. As a result, a space multi-structure chaotic attractor is formed in the TM-HNN. For example, when M_1=M_2=M_3=2, keeping the above parameter values unchanged, the single-structure attractor is reconstructed 6 times along the φ_1-, φ_2-, and φ_3-axes, respectively. The corresponding phase portraits on the φ_1-x_2 plane, φ_2-x_2 plane, and φ_3-x_2 plane are given in Fig.6(a_1), (a_2), and (a_3), respectively. Clearly, the TM-HNN generates a 6×6×6-structure chaotic attractor in φ_1-φ_2-φ_3 phase space. Furthermore, in this case, the dynamical behaviors related to the coupling coefficients are studied. Taking k_1, k_2, and k_3 as adjustable parameters, three groups of different bifurcation diagrams are drawn in Fig.6(b_1),(b_2), and (b_3), respectively. As we can see, that each bifurcation diagram has six clear bar-type areas, which shows that the TM-HNN generates 6-structure chaotic attractors on φ_1-, φ_2-, and φ_3-directions, respectively. Also, it illustrates that the space multi-structure chaotic attractors occur over a wide range. Meanwhile, the corresponding Lyapunov exponents in Fig.6(c_1)-(c_3) further verify the chaos characteristic.

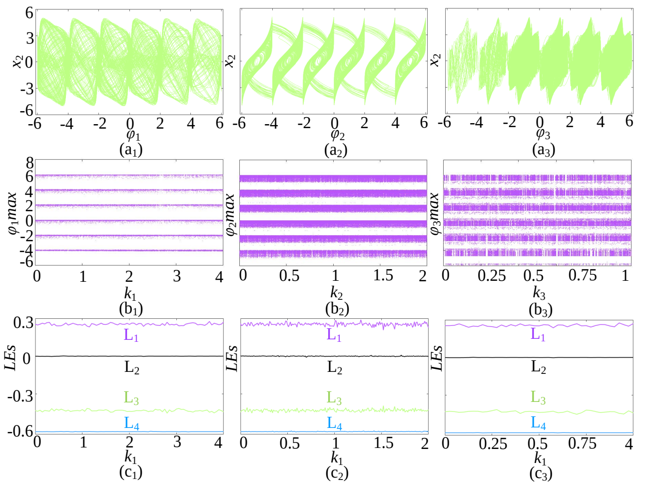

Fig. 6: Dynamical behaviors of the TM-HNN with M_1=M_2=M_3=2. (a_1)-(a_3) Phase portraits on different phase planes of the space 6×6×6-structure chaotic attractor. (b_1)-(b_3) Bifurcation diagram related to parameters k_1, k_2, and k_3, respectively. (c_1)-(c_3) Corresponding Lyapunov exponents (LEs).

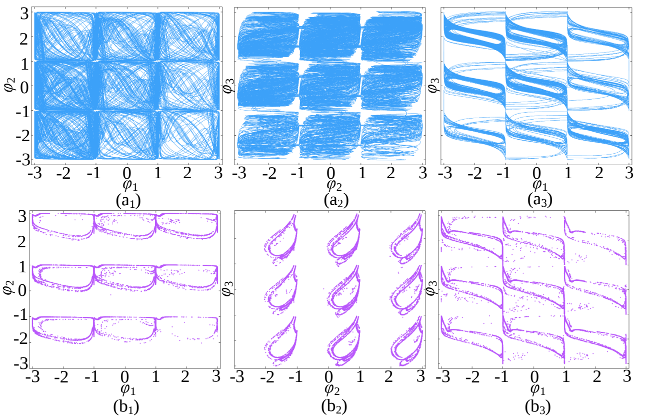

Fig. 7: Phase plane view of the space 3×3×3-structure chaotic attractor. (a_1) Phase portrait on φ_1-φ_2 plane. (a_2) Phase portrait on φ_2-φ_3 plane. (a_3) Phase portrait on φ_1-φ_3 plane. (b_1) Poincaré map on φ_1-φ_2 plane. (b_2) Poincaré map on φ_2-φ_3 plane. (b_3) Poincaré map on φ_1-φ_3 plane.

To further verify the complex dynamical behavior of the space multi-structure attractors, taking control parameters N_1=N_2=N_3=1 as another example, a space 3×3×3-structure chaotic attractor can be obtained from the TM-HNN. Its plane views are shown in Fig.7(a_1)-(a_3). As we can see, the TM-HNN generates 3×3-structure chaotic attractors on φ_1-φ_2, φ_2-φ_3, and φ_1-φ_3 planes, respectively. At the same time, the corresponding Poincaré maps with x_3=0 are drawn in Fig.7(b_1)-(b_3) to further prove the chaos property of the space 3×3×3-structure attractor. The Poincaré maps exhibit complex irregular multi-structure phase trajectories on different phase planes, implying that the TM-HNN generates extremely complex space multi-structure chaotic attractors. Furthermore, different numbers of space multi-structure chaotic attractors in φ_1-φ_3-φ_2 phase space are obtained with different control parameters, as shown in Fig.8. Fig.8 shows that the number of the structure on φ_1-, φ_2-, and φ_3-directions can be easily controlled by control parameters N_1/M_1, N_2/M_2, and N_3/M_3, respectively. And the number of the space multi-structure chaotic attractors is ((2N_1+1) or (2M_1+2))×((2N_2+1) or (2M_2+2))×((2N_3+1) or (2M_3+2)). Consequently, the TM-HNN can generate arbitrary number of space multi-structure chaotic attractors.

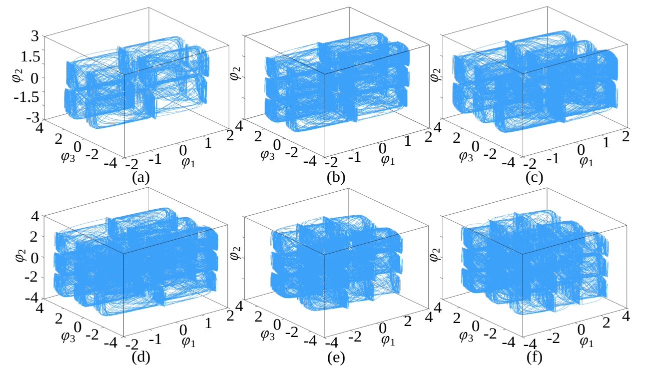

Fig. 8: Phase space view of the space multi-structure chaotic attractors. (a) Space 2×2×2-structure attractor with M_1=M_2=M_3=0. (b) Space 2×3×2-structure attractor with M_1=M_3=0, N_2=1. (c) Space 2×2×3-structure attractor with M_1=M_2=0, N_3=1. (d) Space 2×3×3-structure attractor with N_2=N_3=1, M_1=0. (e) Space 3×3×2-structure attractor with N_1=N_2=1, M_3=0. (f) Space 3×3×3-structure attractor with N_1=N_2=N_3=1.

C. Initial-Related Space Initial-Offset Behaviors

Keeping the parameters b=0.01, k_1=2, k_2=1, k_3=-0.1, d_1=2.42, d_2=4.736, d_3=0.6, unchanged, setting c_1=2, c_2=4, c_3=1, the dynamical characteristic of the initial-offset space coexisting behaviors is investigated by adopting bifurcation diagrams, Lyapunov exponents, phase portraits, and basins of attraction. First, taking M_1=M_2=M_3=3 as an example, three bifurcation diagrams related to initial values φ_{10}, φ_{20}, and φ_{30} as well as their corresponding first four Lyapunov exponents are given in Fig.9. As can be seen in Fig.9(a_1)-(a_3), the bifurcation diagrams exhibit multiple long strip-shaped regions with the same dynamical amplitude but different positions. Each of the long strip regions can evolve to be a single-structure chaotic attractor. Therefore, the position of the chaotic attractors can be controlled by initial states φ_{10}, φ_{20}, and φ_{30}, respectively. In other words, the TM-HNN can generate coexisting chaotic attractors in φ_1-, φ_2-, and φ_3-directions, respectively. When the initial value φ_{10} is set as -1, -3, -5, 1, 3, 5, respectively, and other initial values are fixed as 0.1, the TM-HNN generates coexisting six chaotic attractors on φ_1–direction, as shown in Fig.9(c_1). Adopting a similar method, coexisting six chaotic attractors on φ_2- and φ_3-directions are given in Fig.9(c_2) and (c_3), respectively. And these coexisting chaotic attractors have the same structure but different positions, which have a one-to-one correspondence with the bifurcation diagram in Fig.9(a_1)-(a_3). Fig.9 shows that the TM-HNN can generate coexisting multiple chaotic attractors distributed along the φ_1-, φ_2-, and φ_3-directions, respectively. Therefore, the TM-HNN generates space initial-offset coexisting behaviors.

To further reveal the space characteristic of the initial-offset coexisting behaviors, taking N_1=N_2=N_3=1 as another example, the local attraction basins in the φ_{10}-φ_{20}, φ_{20}-φ_{30}, and φ_{10}-φ_{30} planes are drawn in Fig.10(a_1)-(a_3). It can be seen that each of basin of attraction has nine different regions painted with different colors. Hence, the initial-offset coexisting behavior occurs along φ_{10}, φ_{20}, and φ_{30} directions, simultaneously. Namely, the TM-HNN exhibits space initial-offset coexisting behaviors. Meanwhile, by setting (φ_{10}, φ_{20}, φ_{30})=(-2/0/2, -2/0/2, -2/0/2), coexisting nine chaotic attractors can be obtained in the φ_1-φ_2, φ_2-φ_3, and φ_1-φ_3 plane, respec-

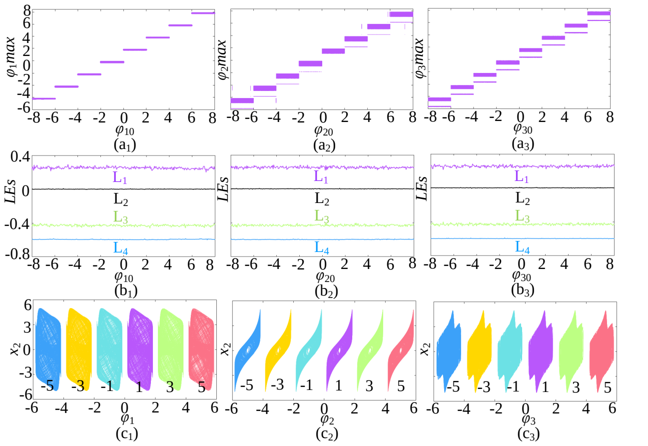

Fig. 9: Dynamical behaviors related to initial states of the TM-HNN with M_1=M_2=M_3=3. (a_1)-(a_3) bifurcation diagrams related to initial values φ_{10}, φ_{20}, and φ_{30}, respectively. (b_1)-(b_3) Corresponding Lyapunov exponents (LEs). (c_1)-(c_3) Phase portraits on different phase planes of the space coexisting 6×6×6 chaotic attractors.

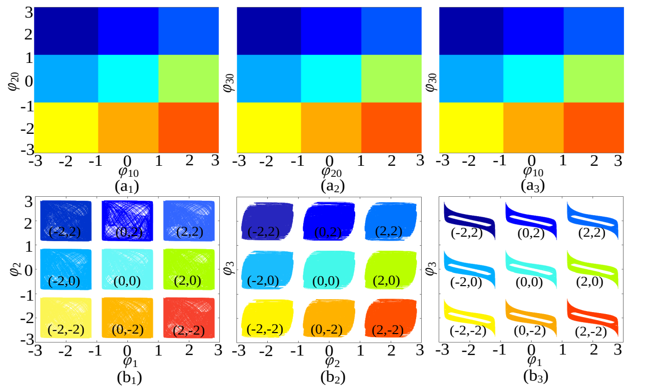

Fig. 10: Basins of attraction and space initial-offset coexisting attractors, where N_1=N_2=N_3=1. (a_1) Basins of attraction on φ_{10}-φ_{20} plane. (a_2) Basins of attraction on φ_{20}-φ_{30} plane. (a_3) Basins of attraction on φ_{10}-φ_{30} plane. (b_1) Space coexisting 3×3×3 attractors on φ_1-φ_2 plane. (b_2) Space coexisting 3×3×3 attractors on φ_2-φ_3 plane. (b_3) Space coexisting 3×3×3 attractors on φ_1-φ_3 plane.

tively, as shown in Fig.10(b_1)-(b_3). Obviously, the positions of the coexisting attractors on φ_1-, φ_2-, and φ_3-directions can be determined by changing initial states φ_{10}, φ_{20}, and φ_{30}, respectively. Accordingly, the TM-HNN generates space initial-offset coexisting behaviors. Moreover, different positions and numbers of space coexisting chaotic attractors in φ_1-φ_3-φ_2 phase space are given with different initial states and control parameters, as shown in Fig.11. To better understand the coexisting behavior, the relationship between the initial values and attractors is given in Table I. Fig.11 shows that the position and number of the coexisting attractors can be controlled by changing the memristors' initial conditions and control parameters, respectively.

IV. Hardware verification And application

In this section, a digital hardware platform based on FPGA is developed for physically implementing the proposed TM-HNN to verify its various dynamical behaviors. Subsequently, the TM-HNN is applied in the pseudorandom number generator.

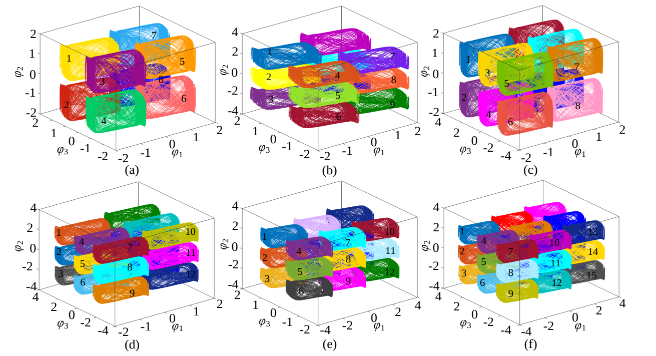

Fig. 11: Phase space view of the space initial-offset coexisting behaviors. (a) Space coexisting 2×2×2 attractors with M_1=M_2=M_3=0. (b) Space coexisting 2×3×2 attractors with M_1=M_3=0, N_2=1. (c) Space coexisting 2×2×3 attractors with M_1=M_2=0, N_3=1. (d) Space coexisting 2×3×3 attractors with N_2=N_3=1, M_1=0. (e) Space coexisting 3×3×2 attractors with N_1=N_2=1, M_3=0. (f) Space coexisting 3×3×3 attractors with N_1=N_2=N_3=1.

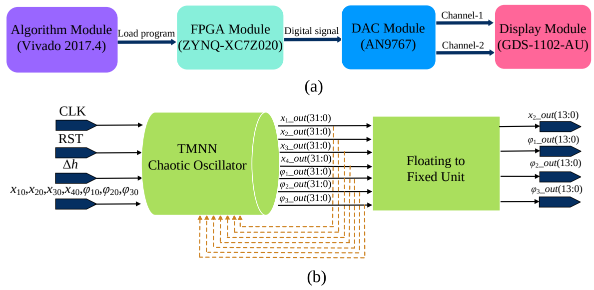

Fig. 12: FPGA-based digital hardware platform. (a) Block diagram of the hardware platform. (b) Flow diagram of the TM-HNN implementation.

A. FPGA-Based Hardware Implementation

Due to the hyperbolic tangent nonlinearity, the hardware implementation of the TM-HNN using an analog circuit is extremely complex. Additionally, the space initial-offset coexisting behaviors in the TM-HNN are highly dependent on the initial states, but the initial states can not be preconfigured in the analog circuit. Different from the analog circuit, the initial states in the digital circuits based on FPGA can be controlled accurately by the software [55]. Thus, the TM-HNN is implemented by using FPGA technology. As shown in Fig.12(a), the block diagram of the FPGA hardware platform is composed of four parts: algorithm module, FPGA module, DAC module, and display module. Among them, the function of the algorithm module is to solve the TM-HNN. The function of the FPGA module is to implement the TM-HNN chaotic oscillator. The DAC (digital-to-analog converter) is used to convert digital signals into analog signals. And the display module aims to capture the experimental results with an oscilloscope.

The key step for the FPGA hardware implementation is to numerically solve the TM-HNN in the algorithm module. Here, the TM-HNN is solved by using the fourth-order Runge-Kutta (RK4) algorithm on the Vivado 2017.4 platform. As shown in Fig.12(b), the key step consists of two modules: TM-HNN chaotic oscillator and floating-to-fixed unit. The chaotic oscillator module contains four input signals and seven output signals, where the system clock "CLK" and the reset signal "RST" are two 1-bit control signals, h and the initial values (x_{10}, x_{20}, x_{30}, x_{40}, φ_{10}, φ_{20}, φ_{30}) are both 32-bit input signals. The seven 32-bit output signals (x_1_out, x_2_out, x_3_out, x_4_out,

TABLE I: THE RELATIONSHIP BETWEEN ATTRACTORS AND INITIAL VALUES.

Initial values-φ_{10}	-1	1	0	-2	2
Attractors	(a)-(1-4); (b)-(1-6); (c)-(1-6); (d)-(1-9)	(a)-(5-8); (b)-(7-9); (c)-(7-8); (d)-(10-12)	(e)-(7-9); (f)-(10-12)	(e)-(1-6); (f)-(1-9)	(e)-(10-12); (f)-(13-15)
Initial values-φ_{20}	-1	1	0	-2	2
Attractors	(a)-(2,4,6,8); (c)-(2,4,6,8)	(a)-(1,3,5,7); (c)-(1,3,5,7)	(b)-(2,5,8); (d)-(2,5,8,11); (e)- (2,5,8,11); (f)-(2,5,8,11,14)	(b)-(3,6,9); (d)-(3,6,9,12); (e)-(3,6,9,12); (f)-(3,6,9,12,15)	(b)-(1,4,7); (d)-(1,4,7,10); (e)-(1,4,7,10); (f)-(1,4,7,10,13)
Initial values-φ_{30}	-1	1	0	-2	2
Attractors	(a)-(3-6); (b)-(4-9); (e)-(4-12)	(a)-(1,2,7,8); (b)-(1-3); (e)-(1-3)	(c)-(3-4); (d)-(4-6); (f)-(4-6)	(c)-(5-8); (d)-(7-12); (f)-(7-15)	(c)-(1,2); (d)-(1-3); (f)-(1-3)

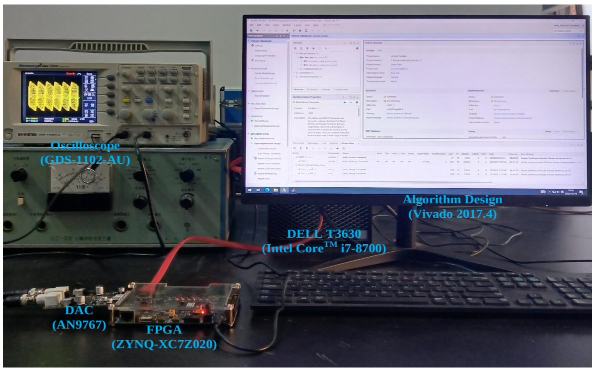

Fig. 13: Hardware implementation devices.

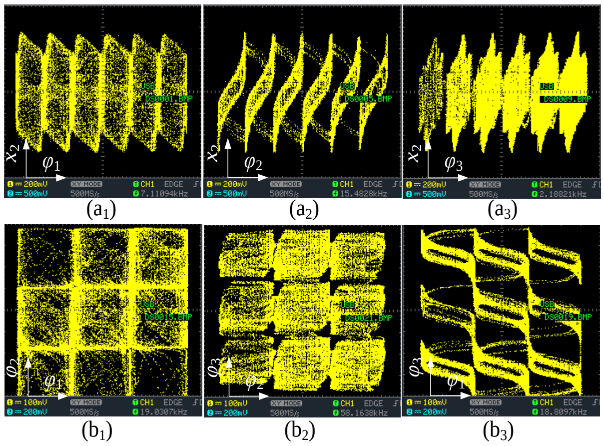

Fig. 14: The experimental results of the space multi-structure attractors. (a_1) Space 6×6×6-structure attractor on φ_1-x_2 plane. (a_2) Space 6×6×6-structure attractor on φ_2-x_2 plane. (a_3) Space 6×6×6-structure attractor on φ_3-x_2 plane. (b_1) Space 3×3×3-structure attractor on φ_1-φ_2 plane. (b_2) Space 3×3×3-structure attractor on φ_2-$\varphi_3$2 plane. (b_3) Space 3×3×3-structure attractor on φ_1-φ_3 plane.

φ_1_out, φ_2_out, φ_3_out) are used as the initial values of the next iteration of the chaotic oscillator. Meanwhile, these output signals are also input to the floating to fixed unit and are further converted into a 14-bit fixed-point number (x_2_out, φ_1_out, φ_2_out, φ_3_out). The two modules are programmed with Verilog HDL language as well as the IP cores of addition, subtraction, multiplication, and hyperbolic tangent operation in Vivado software. The IEEE 754-1985 high precision 32-bit floating point standard is used and the discretization step is set as 0.001.

The proposed TM-HNN is physically realized based on the above digital hardware platform. As shown in Fig.13, the hardware devices contain a workstation (DELL T3630 with Intel CoreTM i7-8700 CPU 3.2GHz), an FPGA development board (Xilinx ZYNQ-XC7Z020), a DAC converter (AN9767) and a digital oscilloscope (GWINSTEK GDS-1102-AU). The developed program is loaded into the FPGA development board, which is connected to the oscilloscope via a DAC converter. The experiment results can be observed from the digital oscilloscope. The experimental results of the space multi-structure chaotic attractors and the space initial-offset coexisting attractors are given in Fig.14 and Fig.15, respectively. It is worth noting that the experimentally captured results are in agreement with those of Fig.6(a_1)-(a_3), Fig.7(a_1)-(a_3), Fig.9(c_1), and Fig.10(b_2) obtained from the Matlab platform. This shows the correctness and feasibility of the FPGA hardware implementation and also provides experimental proof of the proposed TM-HNN.

B. Application in Pseudorandom Number Generators

Chaotic systems are often used to generate pseudorandom numbers in the industrial field [56, 57]. Because the presented TM-HNN can generate chaotic behaviors highly dependent on initial states, it can achieve good performance in this application. Thus, a TM-HNN-based PRNG is designed to investigate its application. First, a chaotic sequence S=(s_1, s_2, $\ldots$, s_n, $\ldots$) is produced by the TM-HNN. Second, each value s_n in S is transformed into a 32-bit float number according to the IEEE 754 float-point standard. Third, the 17th-32nd bits from the float number are truncated as pseudorandom numbers. The designed pseudorandom number generator can be represented by

$$P_i = B(s_n)_{17:32}, \tag{10}$$

where $B(.)$ is to transform a value to be a 32-bit float number. Hence, sixteen binary numbers are produced for each output of the chaotic sequence.

Here, the chaotic sequences generated by the membrane voltages (x_1, x_2, x_3, x_4) in the original HNN and the TM-HNN are used to generate pseudorandom numbers. Firstly, a set of chaotic sequence with length 10^7 are obtained from the original HNN without memristor synapse. Meanwhile, a set of chaotic sequence with length 10^7 are obtained from the space coexisting 3×3×3 attractors in the TM-HNN with initial states (0.1, 0.1, 0.1, 0.1, -2, 2, -2), as shown in Fig.16. Next, according to the above generation method, each set chaotic sequence is processed to produce 160 binary sequences with 10^6 bits, where the first 10 binary sequences are discarded. Finally, the remaining 150 binary sequences are used for

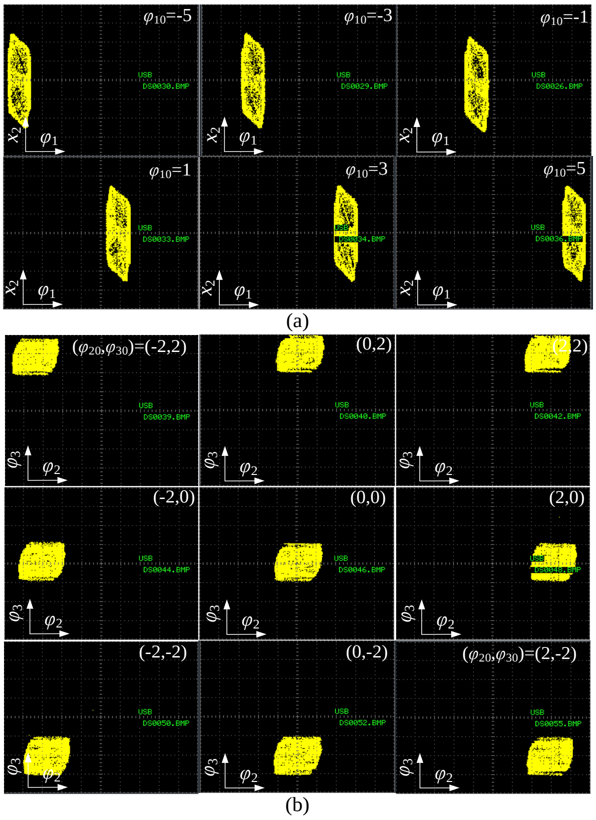

Fig. 15: The experimental results of the space initial-offset coexisting attractors. (a) Space coexisting 6×6×6 attractors on φ_1-x_2 plane. (b) Space coexisting 3×3×3 attractors on φ_2-φ_3 plane.

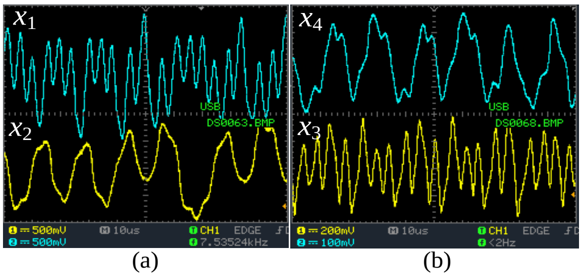

Fig. 16: Four sets of chaotic sequences generated by FPGA-based TM-HNN.

testing. Here, the NIST SP800-22 is used to test the produced random numbers [58]. It is a convinced and all-side test standard that contains 15 sub-tests. In tests, both the P-value larger than 0.01 and the proportion (pro.) larger than 0.96 are considered to pass the related sub-test. Table II lists the test results of the chaotic sequences in the original HNN and TM-HNN. One can see that the results generated by the original HNN can not pass the test because the proportion of the subtests 2, 6, and 15 is less than 0.96. However, the TM-HNN can pass all the sub-tests of the NIST SP800-22 test suite. This means that the TM-HNN produces random numbers with higher randomness. Thus, the proposed TM-HNN has complex chaotic behavior and can be further applied in chaos-based engineering scenarios, such as security communication [59], signal detection [60], and so on.

TABLE II: NIST SP800-22 TEST RESULTS FOR THE ORIGINAL HNN AND TM-HNN

No.	Sub-tests	HNN		TM-HNN	
		P-value	Pro.	P-value	Pro.
1	Frequency	0.5341	0.98	0.8343	0.99
2	Block Frequency	0.0098	0.95	0.8677	0.99
3	Cum.Sums*(F)	0.4559	0.98	0.8343	0.99
	Cum.Sums*(R)	0.7531	0.98	0.4195	0.99
4	Runs	0.5207	0.98	0.6579	1.00
5	Longest Runs	0.2075	0.99	0.5493	1.00
6	Rank	0.8284	0.94	0.2757	0.99
7	FFT	0.2896	0.98	0.9943	0.98
8	Non-Ovla.Temp.*	0.3191	0.98	0.5544	0.99
9	Ovla.Temp.	0.6717	0.98	0.9879	1.00
10	Universal	0.2450	0.98	0.7792	0.98
11	Appr.Entropy	0.9199	0.99	0.7598	1.00
12	Ran.Exc.*	0.3325	0.99	0.3541	0.99
13	Ran.Exc.Var.*	0.4071	0.99	0.5954	0.99
14	Serial (1st)	0.2803	0.98	0.6579	0.99
	Serial (2nd)	0.9357	0.98	0.2622	0.99
15	Linear Complexity	0.0076	0.92	0.4373	0.99

V. Conclusion

Memristors can be used to construct memristive neural networks closer to biological nervous systems. In this paper, we first design a multistable locally active memristor, then present a TM-HNN by using three of the designed memristors to emulate three coupled neural synapses in an HNN with four neurons. The dynamical behaviors of the proposed TM-HNN are investigated by theoretical analysis and numerical simulation. Research results show that the TM-HNN not only can generate space multi-structure chaotic attractors, but also can exhibit space initial-offset coexisting behaviors. Particularly, the number of the space multi-structure attractors and the position of the space coexisting attractors can be flexibly controlled by switching the memristor' control parameters and initial conditions, respectively. Meanwhile, the space multi-structure attractors and the space coexisting attractors in the TM-HNN are further verified by the FPGA-based hardware platform. In addition, a pseudorandom number generator is designed to explore the application of the TM-HNN, and the experimental results show that the chaotic sequences generated by the presented TM-HNN have high randomness. Clearly, these special dynamical behaviors in the TM-HNN lead to the emergence of extreme multistability, which could gain much attention for its potential chaos-based applications by providing greater flexibility. Therefore, it is of great importance to explore neural networks with three or more memristor synapses. The dynamical behaviros in the neural networks with more memristive synaptic weights are thus worth further study.

References

[1] H. Korn and P. Faure, "Is there chaos in the brain? II. Experimental evidence and related models," *C R Biol.*, vol. 326, no.9, pp. 787-840, Sep. 2003.

[2] M. Breakspear, "Dynamic models of large-scale brain activity," *Nat Neurosci.*, vol. 20, no. 3, pp. 340-352, 2017.

[3] C. Yang, S. P. Adhikari, H. Kim, "On learning with nonlinear memristor-based neural network and its replication," *IEEE Trans Circuits Syst I Regul Pap.*, vol. 66, no. 10, pp. 3906-3916, 2019.

[4] C. Pan, Q. Hong, X. Wang, "A novel memristive chaotic neuron circuit and its application in chaotic neural networks for associative memory," *IEEE Trans Comput-Aided Des Integr Circuits Syst.*, vol. 40, no. 3, pp. 521-532, 2021.

[5] J. J. Hopfield, "Neural network and physical system with emergent collective computational abilities," *Proc Nat Acad Sc.*, vol. 79, 2554-2558, 1982.

[6] Z. Aram Z, S. Jafari, J. Ma, et al, "Using chaotic artificial neural networks to model memory in the brain," *Commun Nonlinear Sci Numer Simul.*, vol. 44, pp. 449-459, 2017.

[7] D. J. Hemanth, J. Anitha, L. H. Son, et al, " "Diabetic retinopathy diagnosis from retinal images using modified Hopfield neural network," *J Med Syst.*, vol. 42, Art. no. 247, 2018.

[8] C. Li, Y. Yang, X. Yang, et al, " "A tristable locally active memristor and its application in Hopfield neural network," *Nonlinear Dyn.*, vol. 108, no. 2, pp. 1697-1717, 2022.

[9] S. Duan, Z. Dong, X. Hu, et al, "Small-world Hopfield neural networks with weight salience priority and memristor synapses for digit recognition," *Neural Comput Appl.*, vol. 27, no. 4, pp. 837-844, 2016.

[10] D. Jiang, Z. T. Njitacke, J. D. D. Nkapkop, et al, "A new cross ring neural network: Dynamic investigations and application to WBAN," *IEEE Internet Things J.*, vol. 10, no. 8, pp. 7143-7152, 2023.

[11] J. S. Wang, J. Wang, Q. L. Han, "Multivehicle task assignment based on collaborative neurodynamic optimization with discrete Hopfield networks," *IEEE Trans Neural Netw Learn Syst.*, vol. 32, no. 12, pp. 5274-5286, 2021.

[12] B. Bao, C. Chen, H. Bao, et al, "Dynamical effects of neuron activation gradient on Hopfield neural network: Numerical analyses and hardware experiments," *Int J Bifurcat Chaos.*, vol. 29, no. 04, Art. no. 1930010, 2019.

[13] Z. T. Njitacke, C. L. Matze, M. F. Tsotsop, et al, "Remerging feigenbaum trees, coexisting behaviors and bursting oscillations in a novel 3D generalized Hopfield neural network," *Neural Process Lett.*, vol. 52, no. 1, pp. 267-289, 2020.

[14] H. Lin, C. Wang, C. Chen, et al, "Neural bursting and synchronization emulated by neural networks and circuits," *IEEE Trans Circuits Syst I-Regul Pap.*, vol. 68, no. 8, pp. 3397-3410, 2021.

[15] L. Chua, "Memristor-the missing circuit element," *IEEE Trans Circuits Theory.*, vol. 18, no. 5, pp. 507-519, 1971.

[16] D. B. Strukov, G. S. Snider, D. R. Stewart, et al, "The missing memristor found," *Nature.*, vol. 453, no. 7191, pp. 80-83, 2008.

[17] S. P. Adhikari, M. P. Sah, H. Kim, et al, "Three fingerprints of memristor," *IEEE Trans Circuits Syst I-Regul Pap.*, vol. 60, no. 11, pp. 3008-3021, 2013.

[18] Q. Lai, L. Yang, Y. Liu, "Design and realization of discrete memristive hyperchaotic map with application in image encryption," *Chaos Solitons Fractals.*, vol. 165, Art. no. 112781, 2022.

[19] W. Yao, C. Wang, Y. Sun, et al, "Event-triggered control for robust exponential synchronization of inertial memristive neural networks under parameter disturbance," *Neural Network.*, https://doi.org/10.1016/j.neunet.2023.04.024, 2023.

[20] S. Ding, N. Wang, H. Bao, et al, "Memristor synapse-coupled piecewise-linear simplified Hopfield neural network: Dynamics analysis and circuit implementation," *Chaos Solitons Fractals.*, vol. 166, Art. no. 112899, 2023.

[21] Q. Lai, Z. Wan, P. D. K. Kuate, "Generating grid multi-scroll attractors in memristive neural networks," *IEEE Trans Circuits Syst I-Regul Pap.*, vol. 70, no. 3, pp. 1324-1336, 2023.

[22] H. Lin, C. Wang, F. Yu, et al, "A review of chaotic systems based on memristive Hopfield neural networks," *Mathematics.*, vol. 11, no. 6, Art. no. 1369, 2023.

[23] Q. Lai, C. Lai, P. D. K. Kuate, et al., "Chaos in a simplest cyclic memristive neural network," *Int J Bifurcat Chaos.*, vol. 32, no. 03, Art. no. 2250042, 2022.

[24] X. Hu, C. Liu, L. Liu, et al, "Chaotic dynamics in a neural network under electromagnetic radiation," *Nonlinear Dyn.*, vol. 91, no. 3, pp. 1541-1554, 2018.

[25] F. Yu, H. Shen, Z. Zhang, et al, "Dynamics analysis, hardware implementation and engineering applications of novel multi-style attractors in a neural network under electromagnetic radiation," *Chaos Solitons Fractals.*, vol. 152, Art. No. 111350, 2021.

[26] C. Chen, F. Min, Y. Zhang, et al, "Memristive electromagnetic induction effects on Hopfield neural network," *Nonlinear Dyn.*, vol. 106, no. 3, pp. 2559-2576, 2021.

[27] Y. Leng, D. Yu, Y. Hu, et al, "Dynamic behaviors of hyperbolic-type memristor-based Hopfield neural network considering synaptic crosstalk," *Chaos.*, vol. 30, no. 3, Art. no. 033108, 2020.

[28] D. Ding, H. Xiao, Z. Yang, et al, "Coexisting multi-stability of Hopfield neural network based on coupled fractional-order locally active memristor and its application in image encryption," *Nonlinear Dyn.*, vol. 108, no. 4, pp. 4433-4458, 2022.

[29] T. Dong, X. Gong, T. Huang, "Zero-Hopf bifurcation of a memristive synaptic Hopfield neural network with time delay," *Neural Networks.*, vol. 149, pp. 146-156, 2022.

[30] S. Ding, N. Wang, H. Bao, et al, "Memristor synapse-coupled piecewise-linear simplified Hopfield neural network: Dynamics analysis and circuit implementation," *Chaos Solitons Fractals.*, vol. 166, Art. no.112899, 2023.

[31] H. Lin, C. Wang, L. Cui, et al, "Hyperchaotic memristive ring neural network and application in medical image encryption," *Nonlinear Dyn.*, vol. 110, no. 1, pp. 841-855, 2022.

[32] I. S. Doubla, B. Ramakrishnan, Z. N. Tabekoueng, et al, "Infinitely many coexisting hidden attractors in a new hyperbolic-type memristor-based HNN," *Eur Phys J Spec Top.*, vol. 231, pp. 2371-2385, 2022.

[33] F. Parastesh, S. Jafari, H. Azarnoush, et al, "Chimera in a network of memristor-based Hopfield neural network," *Eur Phys J Spec Top.*, vol. 228, no. 10, pp. 2023-2033, 2019.

[34] Q. Wan, F. Li, S. Chen et al, "Symmetric multi-scroll attractors in magnetized Hopfield neural network under pulse controlled memristor and pulse current stimulation," *Chaos, Solitons Fractals.*, vol. 169, Art. no. 113259, 2023.

[35] C. Chen, F. Min, "ReLU-type memristor-based Hopfield neural network," *Eur Phys J Spec Top.*, vol. 231, no. 16, pp. 2979-2992, 2022.

[36] N. Wang, C. Li, H. Bao, et al, "Generating multi-scroll Chua's attractors via simplified piecewise-linear Chua's diode," *IEEE Trans Circuits Syst I-Regul Pap.*, vol. 66, no. 12, pp. 4767-4779, 2019.

[37] Q. Hong, Y. Li, X. Wang, et al, "A versatile pulse control method to generate arbitrary multidirection multibutterfly chaotic attractors," *IEEE Trans Comput-Aided Des Integr Circuits Syst.*, vol. 38, no. 8, pp. 1480-1492, 2018.

[38] H. Lin, C. Wang, W. Yao, et al, "Chaotic dynamics in a neural network with different types of external stimuli," *Commun Nonlinear Sci Numer Simul.*, vol. 90, Art. no.105390, 2020.

[39] R. Li, E. Dong, J. Tong, et al, "A novel multiscroll memristive Hopfield neural network," *Int J Bifurcat Chaos.*, vol. 32, no. 09, Att. no. 2250130, 2022.

[40] F. Yu F, Shen H, Yu Q, et al, "Privacy protection of medical data based on multi-scroll memristive Hopfield neural network," *IEEE Trans Netw Sci Eng.*, vol. 10, no. 2, pp. 845-858, 2023.

[41] Lai Q, Wan Z, Zhang H, et al, "Design and analysis of multiscroll memristive hopfield neural network with adjustable memductance and application to image encryption," *IEEE Trans Neural Netw Learn Syst.*, early access, Feb. 10, 2022, doi: 10.1109/TNNLS.2022.3146570.

[42] Lin H, Wang C, Sun Y, et al, "Generating n-scroll chaotic attractors from a memristor-based magnetized hopfield neural network," *IEEE Trans Cir Sys-II: Brief Papers.*, vol. vol. 70, no. 1, pp. 311-315, 2023.

[43] F. Yu, X. Kong, A. A. M. Mokbel, et al, "Complex dynamics, hardware implementation and image encryption application of multiscroll memeristive Hopfield neural network with a novel local active memeristor," *IEEE Trans Cir Sys-II: Brief Papers.*, vol. 70, no. 1, pp. 326-330, 2023.

[44] H. Lin, C. Wang, C. Xu, et al, "A memristive synapse control method to generate diversified multi-structure chaotic attractors," *IEEE Trans Comput-Aided Des Integr Circuits Syst.*, vol. 42, no. 2, pp. 942-955, 2023.

[45] S. Zhang, C. Li, J. Zheng, et al, "Generating any number of initial offset-boosted coexisting chua's double-scroll attractors via piecewise-nonlinear memristor," *IEEE Trans Ind Electron.*, vol. 69, no. 7, pp. 7202-7212, 2022.

[46] H. Bao, Z. Hua, N. Wang, et al, "Initials-boosted coexisting chaos in a 2-D sine map and its hardware implementation," *IEEE Trans Industr Inform.*, vol. 17, no. 2, pp. 1132-1140, 2021.

[47] S. Zhang, J. Zheng, X. Wang, et al, "Initial offset boosting coexisting attractors in memristive multi-double-scroll Hopfield neural network," *Nonlinear Dyn.*, vol. 102, no. 4, pp. 2821-2841, 2020.

[48] I. S. Doubla, B. Ramakrishnan, Z. T. Njitacke, et al, "Hidden extreme multistability and its control with selection of a desired attractor in a non-autonomous Hopfield neuron," *AEU- Int J Electron Commun.*, vol. 144, Art. no. 154059, 2022.

[49] H. Lin, C. Wang, J. Sun, et al, "Memristor-coupled asymmetric neural networks: Bionic modeling, chaotic dynamics analysis and encryption application," *Chaos, Solitons Fractals.*, vol. 166, Art. no. 112905, 2023.

[50] H. Bao, M. Hua, J. Ma, et al, "Offset-control plane coexisting behaviors in two-memristor-based Hopfield neural network," *IEEE Trans Ind Electron.*, vol. 70, no. 10, pp. 10526-10535, 2023.

[51] C. Leon, "Everything you wish to know about memristors but are afraid to ask," *Radioengineering.*, vol. 24, no. 2, pp. 319, 2015.

[52] H. Bao, A. Hu, W. Liu, et al, "Hidden bursting firings and bifurcation mechanisms in memristive neuron model with threshold electromagnetic induction," *IEEE Trans Neural Netw Learn Syst.*, vol. 31, no. 2, pp. 502-511, 2020.

[53] Z. Wen, C. Wang, Q. Deng, et al, "Regulating memristive neuronal dynamical properties via excitatory or inhibitory magnetic field coupling," *Nonlinear Dyn.*, vol. 110, no. 4, pp. 3823-3835, 2022.

[54] Y. Lu, C. Wang, Q. Deng, et al, "The dynamics of a memristor-based Rulkov neuron with the fractional-order difference," *Chinese Physics B.*, vol. 31, p. 060502, 2022.

[55] S. M. Mohamed, W. S. Sayed, A. G. Radwan, et al, "FPGA implementation of reconfigurable CORDIC algorithm and a memristive chaotic system with transcendental nonlinearities," *IEEE Trans Circuits Syst I-Regul Pap*., vol. 69, no. 7, pp. 2885-2892, 2022.

[56] L. Liu, H. Huang, S. Hu, "Lorenz chaotic system-based carbon nanotube physical unclonable functions," *IEEE Trans Comput-Aided Des Integr Circuits Syst*., vol. 37, no. 7, pp. 1408-1421, 2018.

[57] S. Kalanadhabhatta, D. Kumar, K. K. Anumandla, et al, "PUF-based secure chaotic random number generator design methodology," *IEEE Trans Very Large Scale Integr VLSI Syst*., vol. 28, no. 7, pp. 1740-1744, 2020.

[58] A. Rukhin, J. Soto, and J. Nechvatal, *A statistical test suite for random and pseudorandom number generators for cryptographic applications*, National Institute of Standards and Technology (NIST), Special Publication 800-22, Rev. 1a, Apr. 2010.

[59] N. Lin, X. Chen, H. Lu, et al, "Chaotic weights: A novel approach to protect intellectual property of deep neural networks," *IEEE Trans Comput-Aided Des Integr Circuits Syst*., vol. 40, no. 7, pp. 1327-1339, 2020.

[60] S. Liu, Y. Sun, Y. Kang, "A novel E-exponential stochastic resonance model and weak signal detection method for steel wire rope," *IEEE Trans Ind Electron*., vol. 69, no. 7, pp. 7428-7440, 2021.

Hairong Lin (Member, IEEE) received M.S. and Ph.D. degree in information and communication engineering and computer science and technology from Hunan University, China, in 2015 and 2021, respectively. He is currently a postdoctoral research fellow at the College of Computer Science and Electronic Engineering, Hunan University, Changsha, China. He is an associate researcher at the Advanced Communication Technology Key Laboratory of Hunan University. He is a member of the Chaos and Nonlinear Circuit Professional Committee of Circuit and System Branch of China Electronic Society. He has presided over three national and provincial projects, and published more than 40 papers in related international journals, such as IEEE-TIE, IEEE-TII, IEEE-TCAD, IEEE-TCAS-I, IEEE-TCAS-II, Neural Networks, etc.

Dr. Lin is a Guest Editor of the journal of Mathematics from 2022 to present. He is also a Guest Editor of the journal of Frontiers in Physics from 2022 to present. Furthermore, he is a regular reviewer for many international journals, such as IEEE-TII, IEEE-TCAS-I, IEEE-TCAS-II, ND, CSF, Chaos, etc. His research interests include memristive neural networks, chaotic systems and circuits, medical image encryption, and neuromorphic engineering.

Chunhua Wang received the M.S. degree from Zhengzhou University, Zhengzhou, China, in 1994, and the Ph.D. degree from Beijing University of Technology, Beijing, China, in 2003. He is currently a Professor of College of Information Science and Engineering, Hunan University, Changsha, China. He is a Doctor tutor, the director of advanced communication technology key laboratory of Hunan universities, the member of academic committee of Hunan university, the director of chaos and nonlinear circuit professional committee of circuit and system branch of China electronic society. Now, his research interests include chaotic circuit, memristor circuit, chaotic encryption, neural networks based on memristor, complex network, current-mode circuit. He has presided over 8 national and provincial projects, and published more than 200 papers retrieved by SCI.

Prof. Wang was a recipient of Hunan Natural Science and Technology second prize in 2022. He was named to the Top 2% of Global Scientists in 2021 and 2022, and selected as the Highly Cited Researcher 2022 in Mathematics-field.

Fei Yu received the M.E. and Ph.D. degree from College of Information Science and Engineering, Hunan University, Changsha, China, in 2010 and 2013, respectively. He is currently a distinguished associate professor at School of Computer and Communication Engineering in Changsha University of Science and Technology, Changsha, China. He focuses on nonlinear system and circuit, complex network and their applications.

Qinghui Hong received the B.S degree and M.S degree in electronic science and technology from Xiangtan University, Xiangtan, China, in 2012 and 2015, respectively, and the Ph.D degree in computer system architecture from Huazhong University of Science and Technology, Wuhan, China, in 2019. He is currently an associate professor with college of computer science and electronic engineering, Hunan University, Changsha 410082, China. He has presided over published more than30 SCI papers, including IEEE TNNLS, IEEE TBCS, IEEE TCAD, IEEE TVLSI, IEEE TCAS-I, etc. His current research interests include memristive neural network, brain-like computing circuits and its application to Artificial Intelligence.

Cong Xu received the Bachelor's degree in communications engineering from Hunan City University, Yiyang, China, in 2016, and received the Ph. D degree in computer science and technology from Hunan University, Changsha, China, in 2022. She is current working at the School of Computer and Communication Engineering, Changsha University of Science and Technology, Changsha, China. Her main research interests include memristive neural network, memristor circuit and chaos secure communication.

Yichuang Sun (M'90–SM'99) received the B.Sc. and M.Sc. degrees from Dalian Maritime University, Dalian, China, in 1982 and 1985, respectively, and the Ph.D. degree from the University of York, York, U.K., in 1996, all in communications and electronics engineering. Dr. Sun is currently Professor of Communications and Electronics, Head of Communications and Intelligent Systems Research Group, and Head of Electronic, Communication and Electrical Engineering Division in the School of Engineering and Computer Science of the University of Hertfordshire, UK. He has published over 330 papers and contributed 10 chapters in edited books. His research interests are in the areas of wireless and mobile communications, RF and analogue circuits, microelectronic devices and systems, and machine learning and deep learning.

Professor Sun was a Series Editor of IEE Circuits, Devices and Systems Book Series (2003-2008). He has been Associate Editor of IEEE Transactions on Circuits and Systems I: Regular Papers (2010-2011, 2016-2017, 2018-2019). He is also Editor of ETRI Journal, Journal of Semiconductors, and Journal of Sensor and Actuator Networks. He was Guest Editor of eight IEEE and IEE/IET journal special issues: High-frequency Integrated Analogue Filters in IEE Proc. Circuits, Devices and Systems (2000), RF Circuits and Systems for Wireless Communications in IEE Proc. Circuits, Devices and Systems (2002), Analogue and Mixed-Signal Test for Systems on Chip in IEE Proc. Circuits, Devices and Systems (2004), MIMO Wireless and Mobile Communications in IEE Proc. Communications (2006), Advanced Signal Processing for Wireless and Mobile Communications in IET Signal Processing (2009), Cooperative Wireless and Mobile Communications in IET Communications (2013), Software-Defined Radio Transceivers and Circuits for 5G Wireless Communications in IEEE Transactions on Circuits and Systems-II (2016), and the 2016 IEEE International Symposium on Circuits and Systems in IEEE Transactions on Circuits and Systems-I (2016). He has also been widely involved in various IEEE technical committee and international conference activities.